Nonadiabatic effects in the $H+H_2$ exchange reaction: Accurate quantum dynamics calculations at a state-to-state level

Tian-Shu Chu,[1,2,a)] Ke-Li Han,[1,b)] Marlies Hankel,[3,c)] Gabriel G. Balint-Kurti,[4,d)] Aron Kuppermann,[5,e)] and Ravinder Abrol[5,f)]
[1]*State Key Laboratory of Molecular Reaction Dynamics, Dalian Institute of Chemical Physics, Chinese Academy of Sciences, Dalian 116023, China*
[2]*Institute for Computational Sciences and Engineering, Qingdao University, Qingdao 266071, China*
[3]*Australian Institute for Bioengineering and Nanotechnology, The University of Queensland, Queensland QLD 4072, Australia*
[4]*School of Chemistry, University of Bristol, Bristol BS8 1TS, United Kingdom*
[5]*Division of Chemistry and Chemical Engineering, California Institute of Technology, Pasadena, California 91125, USA*

(Received 11 December 2008; accepted 6 February 2009; published online 8 April 2009)

Real wave packet propagations were carried out on both a single ground electronic state and two-coupled-electronic states of the title reaction to investigate the extent of nonadiabatic effects on the distinguishable-atom reaction cross sections. The latest diabatic potential matrix of Abrol and Kuppermann [J. Chem. Phys. **116**, 1035 (2002)] was employed in the present nonadiabatic quantum state-to-state scattering calculations over a total energy range-from threshold (the zero point of the reagent H_2) to 3.0 eV. Based on the assumption that the hydrogen atoms are distinguishable in the collisions where the inelastic and elastic ones are excluded, no significant nonadiabatic effects have been found in the calculations of the full state-to-state integral and differential cross sections up to a total energy of 3.0 eV for product vibrational levels $v'=0$, 1, 2, 3. Our results therefore confirm the recent and the previous studies of the geometric phase effects in $H+H_2$ employing a different diabatic double many-body expansion potential matrix or a different BKMP2 potential energy surface. © *2009 American Institute of Physics*. [DOI: 10.1063/1.3089724]

I. INTRODUCTION

It is well known that in the fascinating hydrogen exchange reaction system, a conical intersection (CI) occurs between the ground and the first excited states, with a minimum at about 2.7 eV above the minimum of the isolated H_2 well. Due to that, nonadiabatic effects on the underlying reaction dynamics are of great interest to both experimentalists and theoreticians. There are numerous previous studies related to this issue.[1–25] To name a few, the pioneering reactive quantum scattering calculations of Kuppermann and co-workers,[1,2] etc. To date, most state-to-state quantum scattering calculations[2,13–15,17] for the hydrogen exchange reaction and its variants were focused on the impact on reaction probabilities, and integral and differential cross sections (DCSs) of the geometric phase (GP) effect, a nonadiabatic effect associated with the CI, and can affect the reaction dynamics on the lower adiabatic sheet of the two lowest electronic states. Despite the different methodologies employed in those previous calculations to get the dynamics information at a quantum state-to-state level, the strategies to include the nonadiabatic GP effect are quite similar in that either the vector potential[13–15,17] of Mead and Truhlar[26] is introduced into the nuclear Hamiltonian followed by the solution of a generalized Born–Oppenheimer equation, or GP basis functions[1,2] are used in the solution of a standard Born–Oppenheimer equation. In recent works,[22,24,25] a completely different approach has been applied for studying the nonadiabatic effects in the $H+D_2(v=0,j=0)\rightarrow HD(v'=3,j')+D$ and $H+H_2(v=0,j=0)\rightarrow H_2(v',j')+H$ reactions at either a quantum state-to-state level or a non-state-resolved level. The product rotational distributions over a collision energy range of 1.49–1.85 eV in $H+D_2$ (Ref. 22) and the total reactive cross sections up to a total energy of 4.7 eV in $H+H_2$ (Ref. 24) have been computed on the adiabatic sheet and the two-coupled sheets of the double many-body expansion (DMBE) surface of Varandas *et al.*[21] The fully converged state-to-state integral and differential reactive cross sections up to a total energy of 4.5 eV in $H+H_2$ have also been obtained.[25] In these works,[22,24,25] the Schrödinger equation, formulated using an electronically diabatic representation, is solved numerically by propagating the wave function directly on the two-coupled-electronic states, combining with a reactant-product decoupling method[27,25] for extracting the state-to-state dynamical quantities. Within this kind of dynamics method, the nonadiabatic GP effects are implicitly included through the diabatization angle in the electronically diabatic representation and the nonadiabatic effects such as the couplings to the upper sheet are also included in the reaction mechanism.

[a)]Electronic mail: tschu@dicp.ac.cn.
[b)]Author to whom correspondence should be addressed. Electronic mail: klhan@dicp.ac.cn.
[c)]Electronic mail: m.hankel@uq.edu.au.
[d)]Electronic mail: gabriel.balint-kurti@bristol.ac.uk.
[e)]Electronic mail: aron@caltech.edu.
[f)]Electronic mail: abrol@caltech.edu.

The aim of the present article is to describe and present the results of a rigorous distinguishable-atom reactive quantum scattering calculation at a state-to-state level to investigate the nonadiabatic effects including the GP effect in the title reaction for a range of total energies from threshold to 3.0 eV. These calculations assume that the atoms are distinguishable and the wave functions are not Pauli antisymmetrized. In analogy to the work described in Ref. 22, we propagate the initial-state selected wave function on two-coupled diabatic potential energy surfaces to solve the Schrödinger equation, but the corresponding approach to the dynamics employed here is somewhat different from that of Ref. 22. In this work, we use the real wave packet method.[28] In a previous study, Gray *et al.*[29] propagated nonadiabatically the real wave packet on two–coupled-electronic states for $O(^1D)+H_2$ to produce the averaged dynamical quantities (the total reaction probability and the total cross section). Very recently, Hankel *et al.*[30] developed the DIFFREALWAVE code for extracting the state-to-state dynamical quantities on a single electronic state. The DIFFREALWAVE code has been successfully applied to the adiabatic state-to-state quantum calculations of $H+H_2/D_2$,[30,31] $O+HCl$,[32] etc. Here, we incorporate the relevant features of both the above methods into the present real wave packet method for the purpose of investigating the nonadiabaticiy in the title reaction at a quantum state-to-state calculation level. We present here, to the best of our knowledge, the first nonadiabatic quantum state-to-state calculation using the real wave packet approach. By doing so, we also extend our previous nonadiabatic calculations[33] to a more detailed dynamical level.

Both the one-adiabatic-electronic-state and the two-diabatic-coupled-electronic-state scattering calculations are carried out to examine the extent of the nonadiabatic effects in the reaction dynamics of the distinguishable exchange collisions. The state-to-state reaction probabilities, and full distinguishable-atom integral and DCSs and rovibrational product distributions are calculated and then compared for the two sets of calculations. All calculations use the most recent adiabatic/diabatic potential energy surfaces[20] of Abrol and Kuppermann, in which the diabatization angle for the entire dynamically important region of the configuration space including the CI is obtained from accurate *ab initio* first-derivative couplings between the ground and the first excited states of H_3, and is then used to make the adiabatic-to-diabatic transformation for the two-electronic states to produce the 2×2 diabatic potential energy matrix. The features of this diabatic potential matrix and the discussion of the importance of its components for the reactive scattering processes can be found in Ref. 20.

Section II presents the corresponding methodology for propagating the initial wave packet on the two-coupled diabatic potential surfaces with a Chebyshev iteration procedure. In Sec. III, we describe the numerical aspects of the calculations and present the calculated state-to-state distinguishable-atom dynamical quantities. Comparisons are made between the one-electronic-state and the two-coupled-electronic-state calculations and the nonadiabatic effects in the reaction dynamics are discussed under the assumptions that hydrogen atoms are distinguishable in the collisions and that every collision results in the exchange of the hydrogen atoms with the direct scattering channels being excluded. The conclusions are given in Sec. IV.

II. APPROACH TO THE DYNAMICS

A. Initial wave packet construction

The following initial wave packet was first constructed in a grid space using reactant Jacobi coordinates for the convenience of defining an initial rovibrational state (v_0,j_0) of the molecule reactant (hereafter, the superscripts a and c denote the reactant and the product Jacobi coordinates, respectively),

$$\psi(R^a,r^a,\gamma^a,t=0)=\begin{bmatrix}\varphi_1^{J\Omega}(R^a,r^a,\gamma^a,t=0)\\ \varphi_2^{J\Omega}(R^a,r^a,\gamma^a,t=0)\end{bmatrix}=\begin{bmatrix}\dfrac{\sin(\alpha(R^a-R_0))}{\alpha R^a}e^{-ik_0(R^a-R_0)}\phi_{v,j}(r^a,\gamma^a)Y_{j\Omega}(\gamma,0)\\ 0\end{bmatrix}\quad(i_{\text{start}}=1),$$

or

$$=\begin{bmatrix}0\\ \dfrac{\sin(\alpha(R^a-R_0))}{\alpha R^a}e^{-ik_0(R^a-R_0)}\phi_{v,j}(r^a,\gamma^a)Y_{j\Omega}(\gamma,0)\end{bmatrix}\quad(i_{\text{start}}=2).\tag{1}$$

Here, i_{start} denotes the starting electronic state that the wave packet is initially propagated on in the diabatic representation. A detailed description of the nonzero component in these initial wave packets can be found in Refs. 28, 30, and 31. Both the $i_{\text{start}}=1$ and $i_{\text{start}}=2$ nonadiabatic calculations have been carried out for the $H+H_2$ reaction in the present work. However, the results using $i_{\text{start}}=2$ are very small, for example, the magnitude of the total reaction probabilities at the highest total energy for total angular momentum $J=10$ and 15 is 10^{-5}, hence, the $i_{\text{start}}=2$ results are not shown here. In the rest of this paper, calculations labeled "on V_{11} alone" are two-coupled-diabatic-state calculations for which the initial wave packet is the $i_{\text{start}}=1$ packet and the final analysis is carried out using the first component of the final wave

packet, whereas the "V_{22} alone" calculations also use the $i_{start}=1$ initial wave packet but the second component of the final wave packet. Those labeled "summed over V_{11} and V_{22} alone" are the sum of the calculations labeled on V_{11} alone and on V_{22} alone and are equivalent to a single calculation using the initial wave packet given by the column vector right after the first equality in Eq. (1).

Before the wave packet propagation, the following formula is used to transform the initial wave packet to the product Jacobi coordinates,[30]

$$\varphi_i^{J\Omega'}(R^c,r^c,\gamma^c,t=0)=\varphi_i^{J\Omega}(R^a,r^a,\gamma^a,t=0)\times\frac{R^c r^c}{R^a r^a}d^J_{\Omega\Omega'}(\beta)\quad(i=1,2). \tag{2}$$

$d^J_{\Omega\Omega'}(\beta)$ is a reduced Wigner rotation matrix with β being the angle between the R^a and R^c vectors.

B. Real wave packet propagation on two-coupled diabatic potential energy surfaces

In the real wave packet method,[28,30] using the product Jacobi coordinates, the mapped Schrödinger equation is

$$i\hbar\frac{\partial\psi(R^c,r^c,\gamma^c,t)}{\partial t}=f(\hat{H})\psi(R^c,r^c,\gamma^c,t), \tag{3}$$

with

$$f(\hat{H})=-\frac{\hbar}{\tau}\cos^{-1}(\hat{H}_s).$$

Here, $\hat{H}$ is the Hamiltonian of the reactive H_3 system. In the two-coupled-electronic-state scattering calculation, $\hat{H}$ is the matrix

$$\hat{H}=\begin{bmatrix}\hat{V}_{11}+\hat{H}_{\text{tran+}V_{\text{rot}}} & \hat{V}_{12}\\ \hat{V}_{12} & \hat{V}_{22}+\hat{H}_{\text{tran+}V_{\text{rot}}}\end{bmatrix}, \tag{4}$$

which includes the diabatic potential energy matrix of the H_3 system $\begin{bmatrix}V_{11} & V_{12}\\ V_{12} & V_{22}\end{bmatrix}$, and $\hat{H}_{\text{tran+}V_{\text{rot}}}$ represents the other parts of the Hamiltonian excluding the potential energy operator, i.e., the translational operator and the operator associated with angular momenta.[28,30]

Then, it is necessary to scale and shift $\hat{H}$ to get a scaled Hamiltonian $\hat{H}_s$ as follows:

$$\hat{H}_s=a_s\hat{H}+b_s,$$

$$\hat{H}_s=\begin{bmatrix}H^s_{11} & H^s_{12}\\ H^s_{12} & H^s_{22}\end{bmatrix}=\begin{bmatrix}(\hat{V}_{11}+\hat{H}_{\text{tran+}V_{\text{rot}}})a_s+b_s & a_s\hat{V}_{12}\\ a_s\hat{V}_{12} & (\hat{V}_{22}+\hat{H}_{\text{tran+}V_{\text{rot}}})a_s+b_s\end{bmatrix}, \tag{5}$$

TABLE I. Numerical parameters used in the DIFFREALWAVE code for the H+H$_2$ reaction.

Parameter	Value
Product Jacobi coordinate (R) range	$0.2-12.5a_0$
Number of grid points in R	127
Product Jacobi coordinate (r) range	$0.5-13.5a_0$
Number of grid points in r	143
Number of angular grid points	70
Center of initial wave packet (R_0)	$9.0a_0$
Width of the wave packet (α)	8.0
Smoothing of the wave packet (β)	0.5
Initial translational energy	0.7/2.0 eV[a]
Cutoff energy, V_{cut}	0.42
Scaling parameter a_s	0.867 259 734 110 196 2 eV^{-1}
Shifting parameter b_s	−0.991 327 402 658 898 1
Absorption length in R and r	$4.0(4.0)a_0$
Absorption strength	2.0
Propagation time	2500 iteration steps
Ω'_{max}	31

[a]For the low and high-energy calculations below/up 1.8 eV, respectively.

with

$$a_s=\frac{2}{E_{\text{max}}-E_{\text{min}}},\quad b_s=-1-a_sE_{\text{min}}. \tag{6}$$

E_{min} and E_{max} are the lower and upper bounds to the spectrum of $\hat{H}$.[28]

The solution to the mapped Schrödinger equation is achieved by a damped Chebyshev iteration procedure,

$$\begin{bmatrix}q_1(t+\tau)\\ q_2(t+\tau)\end{bmatrix}=\hat{A}\left(-\hat{A}\begin{bmatrix}q_1(t-\tau)\\ q_2(t-\tau)\end{bmatrix}+2\begin{bmatrix}H^s_{11} & H^s_{12}\\ H^s_{12} & H^s_{22}\end{bmatrix}\begin{bmatrix}q_1(t)\\ q_2(t)\end{bmatrix}\right). \tag{7}$$

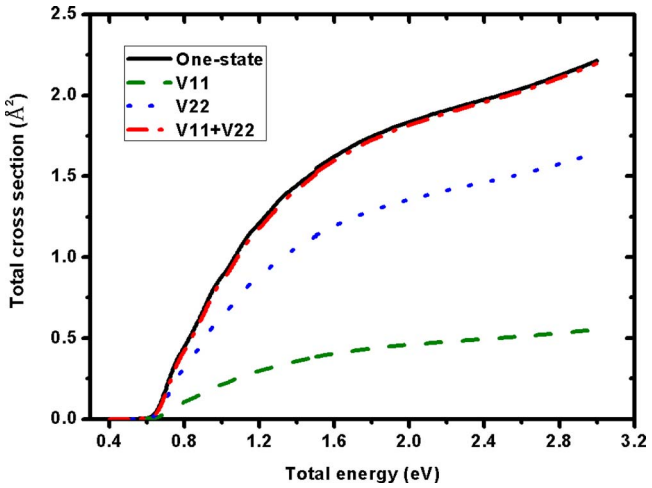

FIG. 1. (Color online) The converged total reaction cross sections as a function of total energy over the range of threshold −3.0 eV for the hydrogen exchange reaction H+H$_2$(v_0=0,j_0=0)→H$_2$+H. The solid line is the result from the one-adiabatic-electronic-state scattering calculation without nonadiabatic effects, the dashed, dotted, and dashed-dotted lines are the results obtained on V_{11}, on V_{22} and the sum over V_{11} and V_{22}, respectively, calculated from the two-coupled-diabatic-electronic-state scattering calculation with nonadiabatic effects. The atoms were assumed distinguishable in all the calculations presented in this paper.

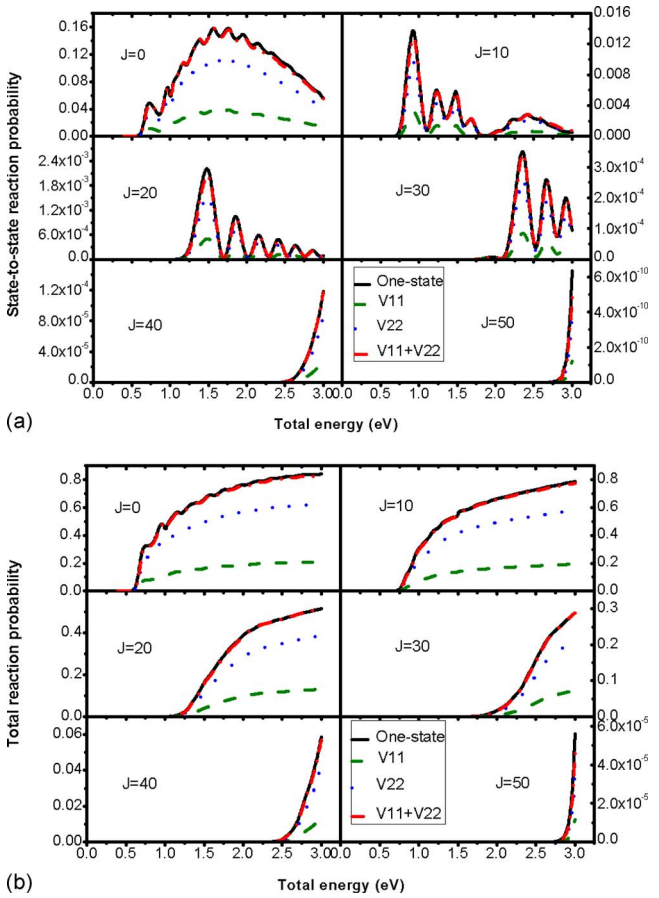

FIG. 2. (Color online) (a) The state-to-state reaction probabilities as a function of total energy in the range of threshold −3.0 eV for the hydrogen exchange reaction $H+H_2(v_0=0,j_0=0)\rightarrow H_2(v'=0,j'=0,\Omega'=0)+H$ with total angular momentum $J=0$, 10, 20, 30, 40, and 50. (b) The corresponding total reaction probabilities as a function of total energy over the range of threshold –3.0 eV summed over all final product states. The solid line is the result from the one-adiabatic-electronic-state scattering calculation without nonadiabatic effects, the dashed, dotted, and dashed-dotted lines are the results obtained on V_{11}, on V_{22} and the sum over V_{11} and V_{22}, respectively, calculated from the two-coupled-diabatic-electronic-state scattering calculation with nonadiabatic effects.

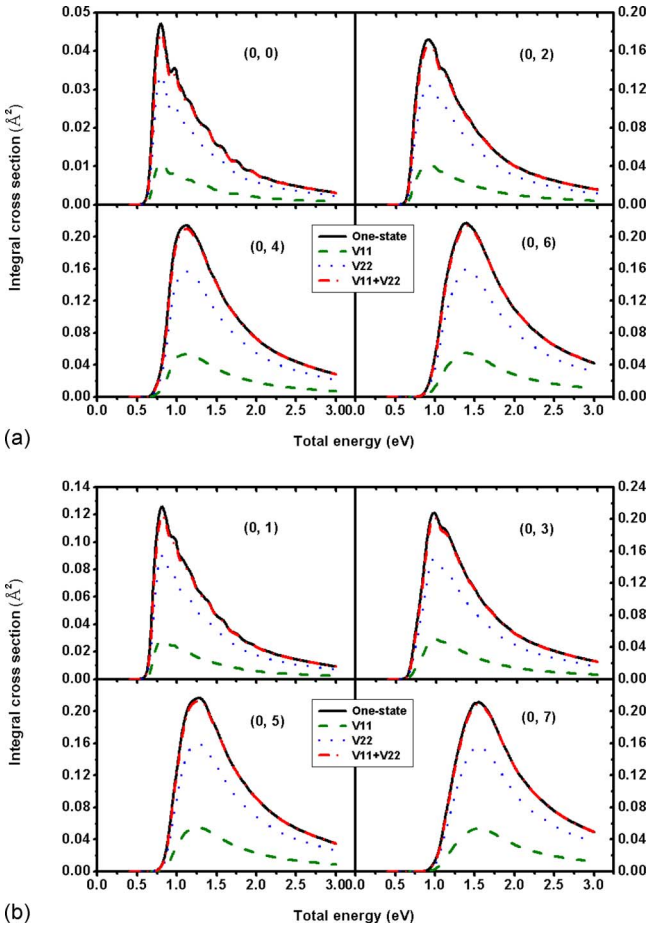

FIG. 3. (Color online) The converged state-to-state ICSs over the total energy range of threshold −3.0 eV. (a) For the product quantum states $v'=0$, $j'=0$, 2, 4, 6. (b) For the product quantum states $v'=0$, $j'=1$, 3, 5, 7. The solid line is the result from the one-adiabatic-electronic-state scattering calculation without nonadiabatic effects, the dashed, dotted, and dashed-dotted lines are the results on V_{11}, on V_{22} and the sum over V_{11} and V_{22}, respectively, calculated from the two-coupled-diabatic-electronic-state scattering calculation with nonadiabatic effects.

Here, $q_i(R^c,r^c,\gamma^c,t)$ $(i=1,2)$ denotes the real part of the wave function $\psi(R^c,r^c,\gamma^c,t)$ at a propagation time t and we omit the coordinate part for simplicity. τ is the time step and is set to 1 a.u. during the propagation. $\hat{A}$ is the damping factor used to absorb the wave packet near the edge of the grid.[28] We note here that the imaginary part of the wave packet is used only once in the first iteration to get $q_i(R^c,r^c,\gamma^c,\tau)$ (see Ref. 28).

C. Derivation of the state-to-state dynamics quantities

Except for the fact that the derivation is performed for each of the two-electronic states starting from $q_1(R^c=R^c_\infty,r^c,\gamma^c,t)$ and $q_2(R^c=R^c_\infty,r^c,\gamma^c,t)$, respectively, there is no difference between the one-electronic-state and the two-coupled-electronic-state scattering calculations for calculating the scattering matrix elements and the subsequent state-to-state integral and DCSs. We therefore left this part unstated and refer to Refs. 28, 30, and 31 for how to extract those state-to-state dynamics quantities and for the other theoretical treatment underlying this dynamics code.

III. RESULTS AND DISCUSSION

The initial state for the quantum scattering calculations were scattering from the ground initial rovibrational state $v_0=0$, $j_0=0$ of H_2 and over the total energy ranged from threshold to 3.0 eV. A cutoff, V_{cut}, was applied to the potential to ensure the efficiency of the DIFFREALWAVE code. Table I lists the numerical parameters used in the present convergence calculations. The present calculations were carried out for total angular momentum $J=0$–50, and with this maximum value of $J=50$ the computed cross sections were fully converged over the investigated energy range. The final state-to-state analysis was implemented for the lowest four vibrational states and the lowest 30 rotational states, but in the calculation of total reaction probabilities and integral cross sections (ICSs) for high energies from 1.8 to 3.0 eV, 7 vibrational states and 51 rotational states are used to obtain the converged results.

Figure 1 presents the converged total reaction cross sections as a function of total energy in the range of threshold to 3.0 eV for the $H+H_2$ $(v_0=0,j_0=0)$ exchange reaction from both the one-adiabatic-electronic-state scattering calculation

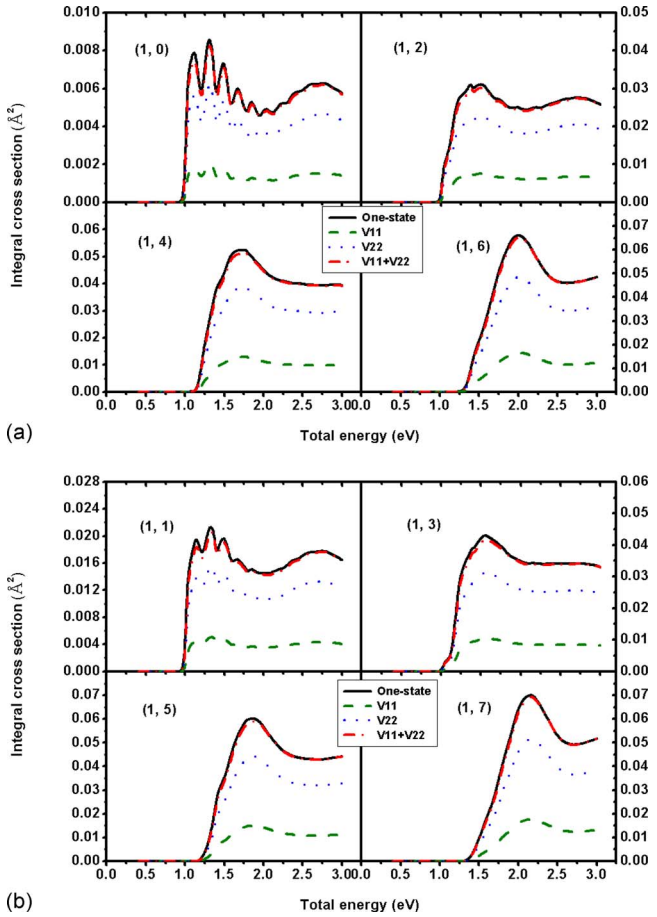

FIG. 4. (Color online) Same as Fig. 3, but for product vibrational state $v'=1$.

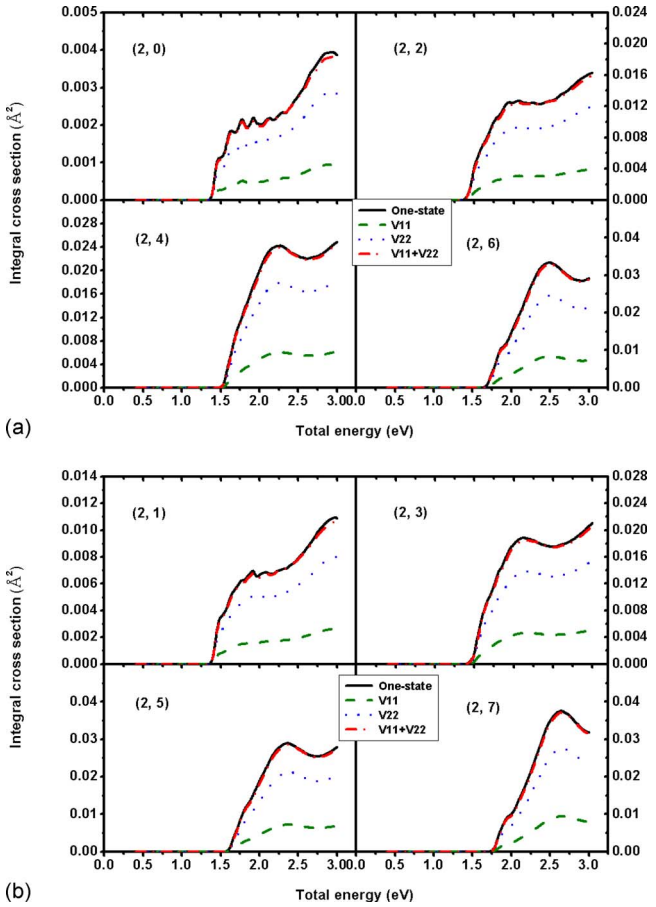

FIG. 5. (Color online) Same as Fig. 3, but for product vibrational state $v'=2$.

(without nonadiabatic effects) and the two-coupled-diabatic-electronic-state scattering calculations (with nonadiabatic effects included). All of the three results generated from the two-coupled-electronic-state calculation, those on V_{11} alone on V_{22} alone and the sum over V_{11} and V_{22}, are shown in the figure. As can be seen, there is very little difference between the two sets of quantum scattering calculations, suggesting a very insignificant role of the nonadiabatic effects in the calculation of the total cross sections up to 3.0 eV. Further comparison of the calculated state-to-state reaction probabilities and total reaction probabilities from the two sets of quantum calculations also reveal no significant effect of the nonadiabatic couplings on these probabilities. Figure 2 plots the state-to-state reaction probabilities from the initial reactant $(v_0=0, j_0=0)$ state to the final product $(v'=0, j'=0, \Omega'=0)$ state as a function of total energy over the range of threshold -3.0 eV for $J=0$, 10, 20, 30, 40, 50, along with the corresponding total $(v_0=0, j_0=0)$ reaction probabilities summing over the final product states. We can see that the $(v_0=0, j_0=0 \rightarrow v'=0, j'=0, \Omega'=0)$ state-to-state and the total reaction probabilities generated from the two-electronic-state calculations are identical to those from the one-electronic-state calculations at most energies for these individual J values, and that the state-to-state reaction probabilities have richer structures than the total reaction probabilities. The previous work of Mahapatra *et al.*[23] demonstrated that inclusion of the upper electronic state has a very small effect on the total reaction probabilities of $H+H_2$, and our results of the reaction probabilities confirmed this finding and extended it to a state-to-state level. The above calculated results are also in accordance with the recent nonadiabatic wave packet study of Jayachander Rao *et al.*[24] on DMBE surface demonstrating a very minor effect of the nonadiabatic couplings on the converged total reaction probabilities and total cross sections up to a total energy of 4.7 eV for $H+H_2$.

The converged state-to-state distinguishable-atom ICSs, summed over all values of omega prime (the quantum number of the component of the diatomic product angular momentum along the direction of its relative velocity vector with respect to the product atom), are shown in Figs. 3–6 for the product vibrational state $v'=0$, 1, 2, and 3, respectively, each with product rotational states $j'=0-7$. As shown, the full ICSs calculated from the two sets of calculations are nearly identical, thus indicating that nonadiabatic effects play a negligible role in calculating the full distinguishable-atom ICSs over the investigated energy range. Figure 7 displays the rotational distributions for $H+H_2(v_0=0, j_0=0) \rightarrow H_2(v'=0-3, j')+H$ at the six total energies 1.8, 2.0, 2.3, 2.5, 2.8, and 3.0 eV summed over all partial waves up to $J=50$. Hereafter, only the results from the one-adiabatic-electronic-state calculation and the sums of the results for V_{11} and V_{22} of the two-coupled-diabatic-electronic-state calculations are shown for a clearer comparison. As expected, there is almost no difference between calculations with and without nonadia-

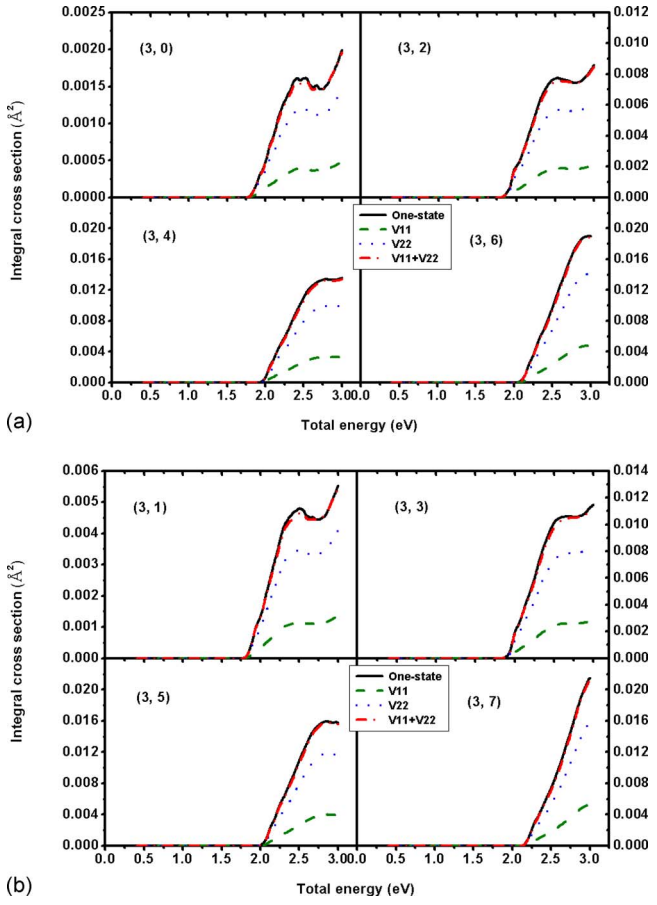

FIG. 6. (Color online) Same as Fig. 3, but for product vibrational state $v'=3$.

batic effects for $v'=0-3$. We therefore say that neither the GP effect nor the couplings to the upper electronic state can influence the state-to-state distinguishable-atom ICSs below the total energy of 3.0 eV. Thus, these results confirmed many previous studies of the GP effect in the title reaction, especially a very recent quantum wave packet state-to-state

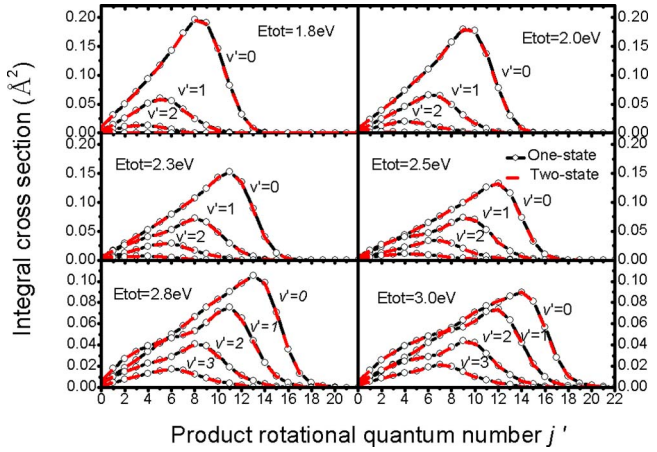

FIG. 7. (Color online) Product rotational distributions for vibrational levels $v'=0$, 1, 2, and 3 at $E_{tot}=1.8$, 2.0, 2.3, 2.5, 2.8, and 3.0 eV. The solid line with open circles is the result from the one-adiabatic-electronic-state scattering calculation without nonadiabatic effects, the dashed line is the result summed over V_{11} and V_{22} from the two-coupled-diabatic-electronic-state scattering calculation with nonadiabatic effects.

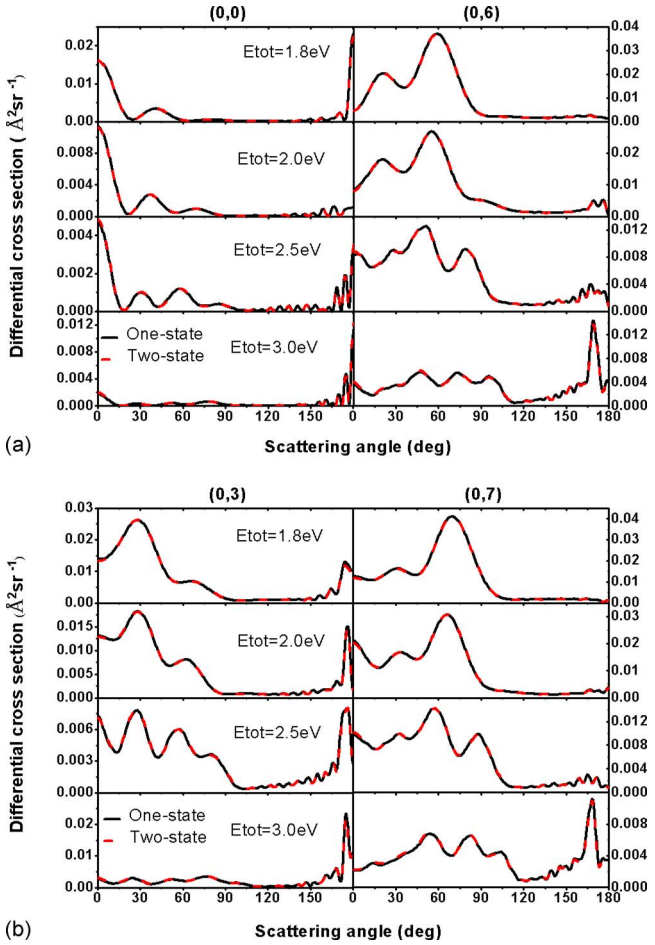

FIG. 8. (Color online) The converged state-to-state DCSs as a function of scattering angle at $E_{tot}=1.8$, 2.0, 2.5, and 3.0 eV for product states $v'=0$, (a) $j'=0$, 6 and (b) $j'=3$, 7. The solid line is the result from the one-adiabatic-electronic-state scattering calculation without nonadiabatic effects, the dashed line is the result summed over V_{11} and V_{22} from the two-coupled-diabatic-electronic-state scattering calculation with nonadiabatic effects.

study,[25] where the converged state-to-state integral and DCSs up to a total energy of 4.5 eV were obtained from calculations with and without GP/nonadiabatic effects.

The full state-to-state distinguishable-atom DCSs at $E_{tot}=1.8$, 2.0, 2.5, and 3.0 eV are plotted versus the scattering angle in Figs. 8–10 for several selected states of the product quantum states $v'=0-3$, $j'=0-7$. The results of Figs. 8(a), 9(a), and 10(a) should not be compared to experiment because they are not Pauli antisymmetrized.[34,35] Such antisymmetrization would involve inclusion of the direct scattering amplitude which, because of interference with the exchange scattering amplitude, would result in oscillations of the observable state-to-state DCSs as a function of scattering angle which would have opposite phases for the one-state and two-coupled-state calculations.[2,35] Ignoring such antisymmetrization effects, comparison of the results displayed in Figs. 8–10 shows once again that there are no significant nonadiabatic effects in the calculation of the distinguishable-atom full DCSs since at most scattering angles the DCSs generated from the two-electronic-state calculations are indistinguishable to those from the one-electronic-state calculations. Comparisons of the calculated DCSs for other product quantum states show a similar behavior and therefore not

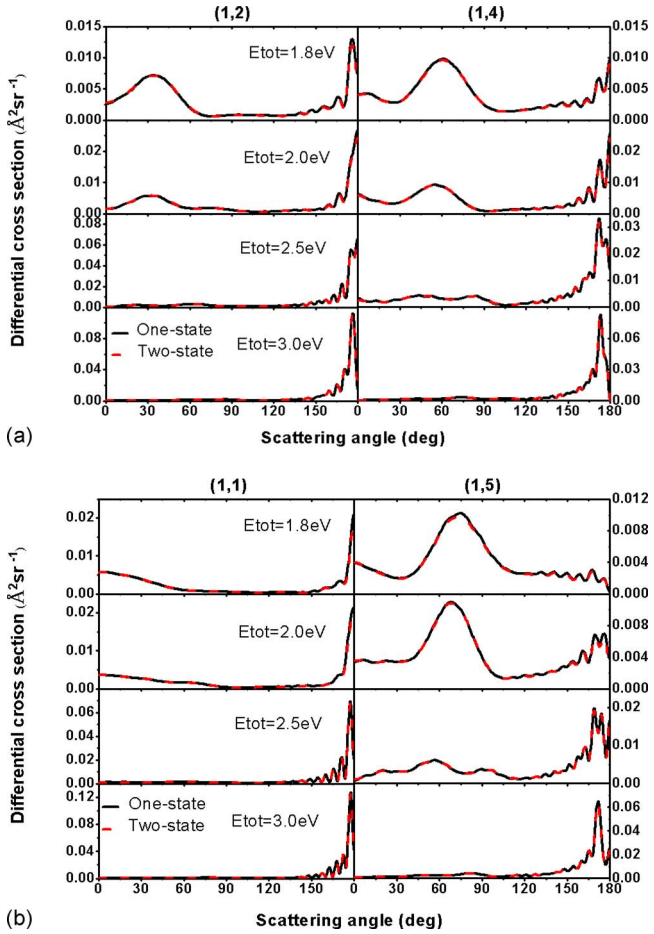

FIG. 9. (Color online) The full state-to-state DCSs as a function of scattering angle at E_{tot}=1.8, 2.0, 2.5, and 3.0 eV for product states v'=1, (a) j'=2, 4 and (b) j'=1, 5. The solid line is the result from the one-adiabatic-electronic-state scattering calculation without nonadiabatic effects, the dashed line is the result summed over V_{11} and V_{22} from the two-coupled-diabatic-electronic-state scattering calculation with nonadiabatic effects.

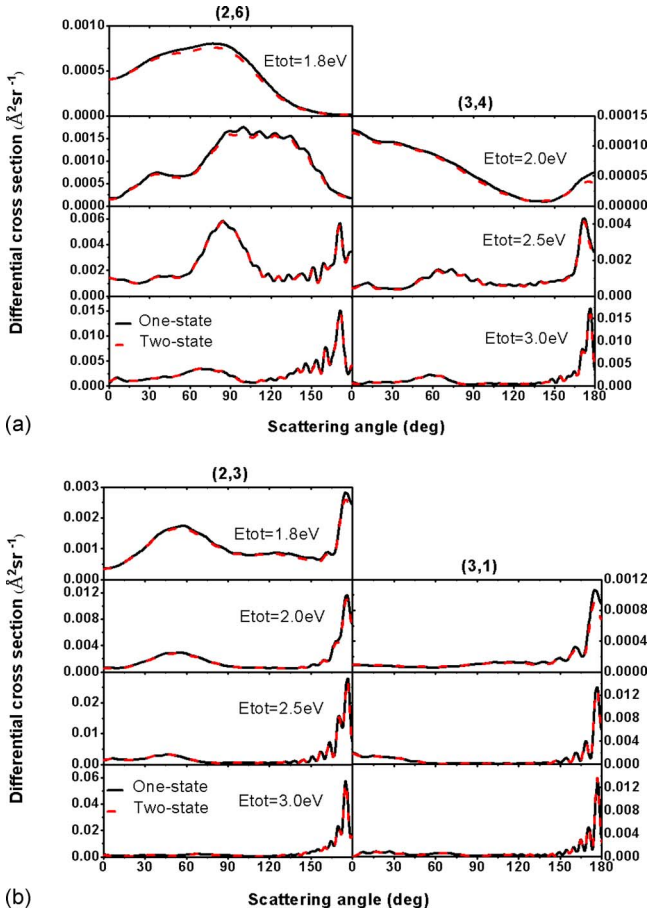

FIG. 10. (Color online) The full state-to-state DCSs as a function of scattering angle at E_{tot}=1.8, 2.0, 2.5, and 3.0 eV for product states (a) v'=2, j'=6; v'=3, j'=4 and (b) v'=2, j'=3; v'=3, j'=1. The solid line is the result from the one-adiabatic-electronic-state scattering calculation without nonadiabatic effects, the dashed line is the result summed over V_{11} and V_{22} from the two-coupled-diabatic-electronic-state scattering calculation with nonadiabatic effects.

shown here. In Fig. 11, we plotted the distinguishable-atom DCSs versus total energy at three scattering angles 0°, 90°, and 180° for several product states (0,0), (1,0), (1,1), (2,0), and (2,6), (2,7), (3,4), (3,7). As can be seen, despite some noticeable high-energy differences at the scattering angle 0° for product states (1,0), (2,6), (2,7), the two sets of calculations demonstrated very small differences, and this further evidenced the very minor nonadiabatic effects on most of the calculated state-to-state distinguishable-atom DCSs. The behaviors of the DCSs reported here are in a qualitative agreement with those in Ref. 25.

Given that the present real wave packet calculation employs a different potential matrix from the DMBE potential matrix used in the recent quantum studies,[22,24,25] the agreement with those previous studies in predicting an insignificant role of the GP effect and the upper electronic state in calculating the state-resolved and the non-state-resolved dynamical quantities with total energies up to 3.0 eV, has presented here a useful confirmation of the previous studies, since there was always a lingering doubt that the nonparticipation of the upper state might be an artifact of the DMBE potential.

Finally, we note here that the present quantum real wave packet calculations are performed with the above-mentioned assumption that leads to only the distinguishable-atom ICSs and DCSs. However, it would be interesting to know the extent of the nonadiabatic effects including the GP effect on the indistinguishable-atom ICSs and DCSs since the physically measurable cross sections for H+H_2 are indistinguishable-atom ones, where the interference between the exchange and the direct amplitudes is implicated in the para-para (even j to even j') and ortho-ortho (odd j to odd j') transition cross sections.[34,35] Whenever the interference between the reactive and nonreactive amplitudes is significant in such kind of transition cross sections, the GP effect is predicted and reported to be significant.[15,26] Further investigation of the nonadiabatic effects on the para-para and ortho-ortho ICSs and DCSs requires that the wave packet calculations be carried out to perform the state-to-state analysis for the direct (the nonreactive) scattering channels, and this will be the subject of our future work.

IV. CONCLUSIONS

In this article, we presented a real wave packet approach that can be applied to the nonadiabatic quantum state-to-state

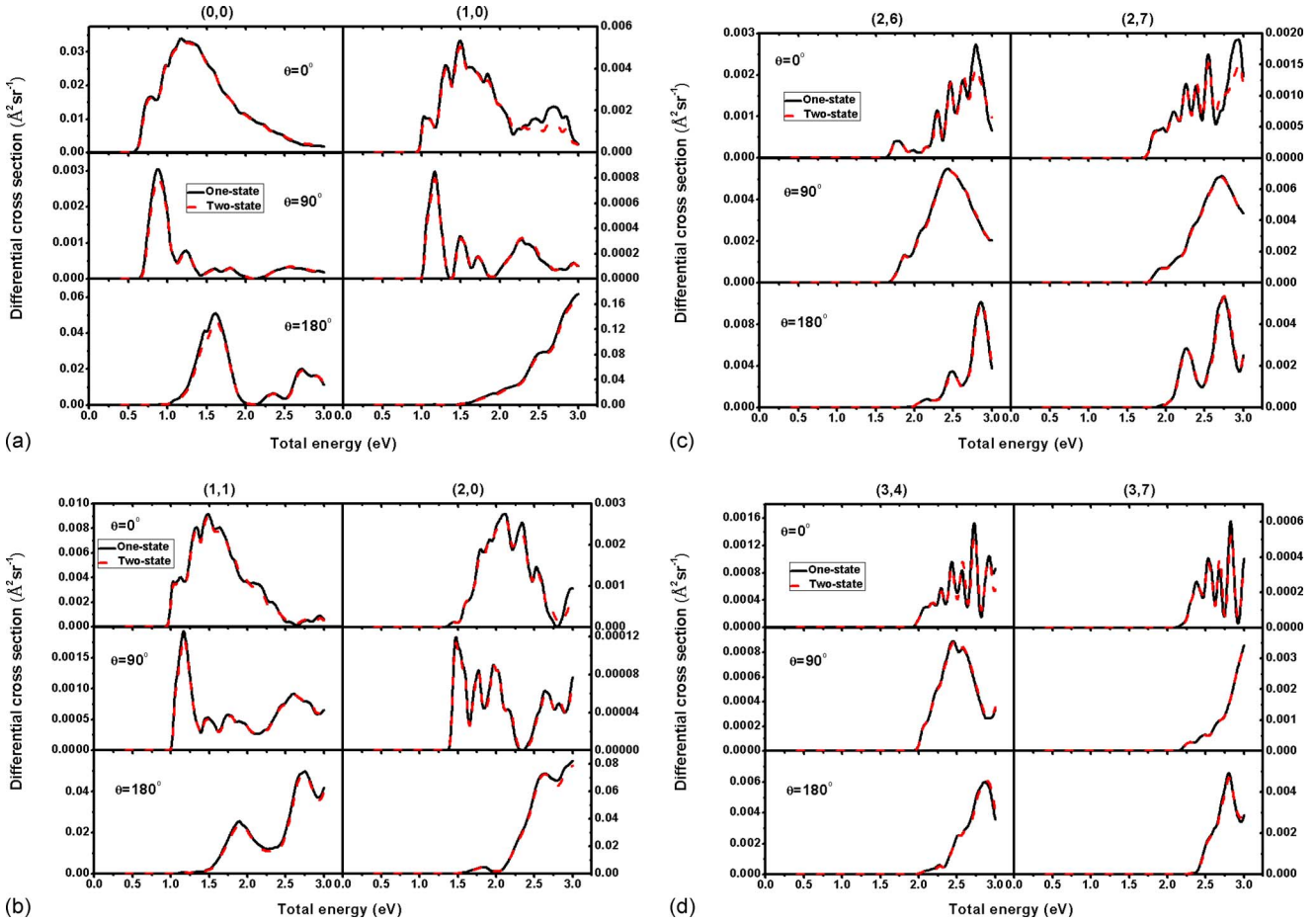

FIG. 11. (Color online) The converged state-to-state DCSs as a function of total energy over the total energy range of threshold −3.0 eV at three scattering angles 0°, 90°, and 180° for eight product states (0,0), (1,0), (1,1), (2,0), and (2,6), (2,7), (3,4), (3,7). The solid line is the result of the one-adiabatic-electronic-state scattering calculation without nonadiabatic effects, the dashed line is the result summed over V_{11} and V_{22} from the two-coupled-diabatic-electronic-state scattering calculation with nonadiabatic effects.

scattering calculations of chemical exchange reactions. By using this method, we have carried out accurate quantum scattering calculations for the distinguishable-atom hydrogen exchange reaction $H+H_2(v_0=0,j_0=0)\rightarrow H_2(v'=0-3,j'=0-7)+H$ to obtain converged state-to-state reaction probabilities, integral, and DCSs (summed over the product diatom rotational projection quantum numbers) for the total energy range of threshold −3.0 eV. Both the one-adiabatic-electronic-state and the two-coupled-diabatic-electronic-state scattering calculations were carried out to investigate the nonadiabatic effects in the reaction dynamics. The recent diabatic potential energy surface of Abrol and Kuppermann was employed in the present quantum calculations. The quantum calculation was carried out for total angular momentum $J=0-50$, which yields the fully converged state-to-state integral/DCSs up to 3.0 eV. Comparison of the calculations with and without nonadiabatic effects included has demonstrated that there are no significant nonadiabatic effects in the full state-to-state distinguishable-atom ICSs up to 3.0 eV for the product vibrational states $v'=0-3$. It is also found that in the calculations of the distinguishable-atom full DCSs, effect of nonadiabatic couplings is too much insignificant at most product states and most energies. Our calculations supported many other previous theoretical studies of the GP effect in $H+H_2$ and its isotopic variants. In addition, it is necessary to extend the present state-to-state reactive quantum scattering calculations to the state-to-state nonreactive scattering calculations for the purpose to study the influence of the nonadiabatic effects on the indistinguishable-atom integral and DCSs of $H+H_2$, which is an important issue in advancing our understanding of the nonadiabatic effects on the reaction dynamics of this hydrogen collision system.

ACKNOWLEDGMENTS

This work was supported by the NSFC (Grant Nos. 2083308, 20633070, and 10874096) and QDUF (Grant No. 063-06300510). One of the authors (M.H.) would like to thank The University of Queensland, the Queensland Smart State Research Facilities Fund and Sun Microsystems for funding.

[1] B. Lepetit and A. Kuppermann, Chem. Phys. Lett. **166**, 581 (1990).
[2] Y.-S. Mark Wu, A. Kuppermann, and B. Lepetit, Chem. Phys. Lett. **186**, 319 (1991).
[3] Y.-S. Mark Wu, A. Kuppermann, and J. B. Anderson, Phys. Chem. Chem. Phys. **1**, 929 (1999).
[4] R. Abrol, A. Shaw, A. Kuppermann, and D. R. Yarkony, J. Chem. Phys. **115**, 4640 (2001).
[5] E. E. Marinero, C. T. Rettner, and R. N. Zare, Phys. Rev. Lett. **48**, 1323 (1982).

[6] D. Bean, F. Fernández-Alonso, and R. N. Zare, J. Phys. Chem. A **105**, 2228 (2001).
[7] D. Bean, J. D. Ayers, F. Fernández-Alonso, and R. N. Zare, J. Chem. Phys. **116**, 6634 (2002).
[8] J. D. Ayers, A. E. Pomerantz, F. Fernández-Alonso, F. Ausfelder, B. D. Bean, and R. N. Zare, J. Chem. Phys. **119**, 4662 (2003).
[9] A. E. Pomerantz, F. Ausfelder, R. N. Zare, S. C. Althorpe, F. J. Aoiz, L. Bañares, and J. F. Castillo, J. Chem. Phys. **120**, 3244 (2004).
[10] F. Ausfelder, A. E. Pomerantz, R. N. Zare, S. C. Althorpe, F. J. Aoiz, L. Bañares, and J. F. Castillo, J. Chem. Phys. **120**, 3255 (2004).
[11] A. E. Pomerantz, F. Ausfelder, R. N. Zare, J. C. Juanes-Marcos, S. C. Althorpe, V. S. Rábanos, F. J. Aoiz, L. Bañares, and J. F. Castillo, J. Chem. Phys. **121**, 6587 (2004).
[12] K. Koszinowski, N. T. Goldberg, A. E. Pomerantz, R. N. Zare, J. C. Juanes-Marcos, and S. C. Althorpe, J. Chem. Phys. **123**, 054306 (2005).
[13] B. K. Kendrick, J. Chem. Phys. **112**, 5679 (2000); **114**, 4335 (2001).
[14] B. K. Kendrick, J. Chem. Phys. **118**, 10502 (2003).
[15] B. K. Kendrick, J. Phys. Chem. A **107**, 6739 (2003).
[16] D. Dai, C. C. Wang, S. A. Harich, X. Wang, X. Yang, S. D. Chao, and R. T. Skodje, Science **300**, 1730 (2003).
[17] J. C. Juanes-Marcos and S. C. Althorpe, J. Chem. Phys. **122**, 204324 (2005).
[18] J. C. Juanes-Marcos, S. C. Althorpe, and E. Wrede, J. Chem. Phys. **126**, 044317 (2007).
[19] B. Lepetit, R. Abrol, and A. Kuppermann, Phys. Rev. A **76**, 040702 (2007).
[20] R. Abrol and A. Kuppermann, J. Chem. Phys. **116**, 1035 (2002).
[21] A. J. C. Varandas, F. B. Brown, C. A. Mead, D. G. Truhlar, and N. C. Blais, J. Chem. Phys. **86**, 6258 (1987).
[22] R. F. Lu, T. S. Chu, Y. Zhang, K. L. Han, A. J. C. Varandas, and J. Z. H. Zhang, J. Chem. Phys. **125**, 133108 (2006).
[23] S. Mahapatra, H. Köppel, and L. S. Cederbaum, J. Phys. Chem. A **105**, 2321 (2001).
[24] B. Jayachander Rao, R. Padmanaban, and S. Mahapatra, Chem. Phys. **333**, 135 (2007).
[25] F. Bouakline, S. C. Althorpe, and D. P. Ruiz, J. Chem. Phys. **128**, 124322 (2008), and references therein.
[26] C. A. Mead and D. G. Truhlar, J. Chem. Phys. **70**, 2284 (1979); C. A. Mead, *ibid.* **72**, 3839 (1980).
[27] T. Peng and J. Z. H. Zhang, J. Chem. Phys. **105**, 6072 (1996).
[28] S. K. Gray and G. G. Balint-Kurti, J. Chem. Phys. **108**, 950 (1998).
[29] S. K. Gray, G. G. Balint-Kurti, G. C. Schatz, J. J. Lin, X. H. Liu, S. Harich, and X. M. Yang, J. Chem. Phys. **113**, 7330 (2000).
[30] M. Hankel, S. C. Smith, R. J. Allan, S. K. Gray, and G. G. Balint-Kurti, J. Chem. Phys. **125**, 164303 (2006).
[31] T. S. Chu, K. L. Han, M. Hankel, and G. G. Balint-Kurti, J. Chem. Phys. **126**, 214303 (2007).
[32] H. Yang, K. L. Han, S. Nanbu, H. Nakamura, G. G. Balint-Kurti, H. Zhang, S. C. Smith, and M. Hankel, J. Chem. Phys. **128**, 014308 (2008).
[33] T. S. Chu, Y. Zhang, and K. L. Han, Int. Rev. Phys. Chem. **25**, 201 (2006).
[34] G. C. Schatz and A. Kuppermann, J. Chem. Phys. **65**, 4642 (1976).
[35] G. C. Schatz and A. Kuppermann, J. Chem. Phys. **65**, 4668 (1976).